Paper: IX-2729-2021 (IX-H-916-2021)

Title: **Microstructural changes in 16-8-2 weld metal during exposure to 750°C for extended times**

DB Swanepoel*; Prof. PGH Pistorius†

Abstract
Ever-leaner compositions are targeted for nominal type 16-8-2 weld metals in attempts to limit sigma phase formation during elevated-temperature operation. Three variants of type 16-8-2 weld metals were exposed to aging at 750°C for up to 3500 h. Evaluation of the resultant structures by magnetic measurements, neutron diffraction (at ambient and cryogenic temperatures), and electron backscatter diffraction established that the leaner variants were susceptible to forming martensite after aging. This is ascribed to a local increase in the martensite start temperature due to sensitization taking place during elevated-temperature aging. The extent of martensite formation diminished during aging treatments exceeding 1000 h owing to diffusion of solute elements from the austenitic matrix to the sensitized regions (recovery). Subsequent elevated-temperature aging of the microstructures containing martensite also resulted in a decrease in martensite content: the mechanism, however, differs from that for single-cycle exposure. This observation is explained by martensite reversion to austenite. Martensite formation was completely absent from the higher-alloyed variant. This variant experienced intergranular carbide precipitation and delta ferrite decomposition into secondary austenite and carbides. This work demonstrates significantly different aging responses for composition variants within the allowed ranges for type 16-8-2 weld metals.

Keywords: 16-8-2, sensitization, martensite, delta ferrite

Introduction
Type 16-8-2 weld metal displays the unique ability to produce welds free from solidification cracking under restraint, despite containing very small amounts of residual delta ferrite in the as-welded microstructure [1]. The lean nature of this alloy allows it to solidify as primary delta ferrite, thereby affording it resistance to solidification cracking yet also permits more complete transformation of delta ferrite to austenite during cooling. As-welded Ferrite Numbers (FN) of 0 to 4 are therefore typical for this alloy, which has been proven [2] to be adequate in the prevention of solidification cracking. This alloy composition is beneficial for elevated-temperature service because it displays high creep ductility and resistance to embrittlement due to the small amount of delta ferrite that can transform to the sigma phase [3]. To further reduce sigma-phase formation, compositional changes within the ranges permitted by the Specification for Bare Stainless Steel Welding Electrodes and Rods SFA-5.9 for ER16-8-2 [1] are often made by reducing the Cr and Mo contents [4, 5] and increasing C [5]. In such cases, Ni is also reduced to ensure that primary ferritic solidification is attained. There is hence an increasing trend toward supplying 16-8-2 in leaner compositions.

The lean nature of the alloy, however, places it in close proximity to the martensite boundaries as proposed by Kotecki [6] on the WRC-1992 diagram. Martensite is rarely observed in the as-welded condition, as evidenced by the low magnetic permeability determined by Fischer Feritscope measurements [4, 7]. The C content of these alloys is normally raised to improve its elevated-temperature strength. The formation of $M_{23}C_6$ carbides on the grain boundaries is hence expected during elevated-temperature service. It is postulated [7] that removal of the solute elements (Cr, Mo, and C) during such carbide formation locally raises the martensite start (M_s) temperatures to values that allow the formation of martensite during cooling to ambient temperature. This might typically be the case during shutdown or unintended trips after initial commissioning of elevated-temperature

* Department of Materials Science and Metallurgical Engineering, University of Pretoria, South Africa; niel.swanepoel@sasol.com
† Department of Materials Science and Metallurgical Engineering, University of Pretoria, South Africa; pieter.pistorius@up.ac.za ; https://orcid.org/0000-0001-6582-8157

equipment. Fink et al [8] aged 16-8-2 weld metal (with nominal 14.8%Cr, 7.8%Ni and 1.0%Mo) at 705˚C for 168 h. They found that the FN (measured with a Magne-Gage) increased from 1.7 FN to 9 FN during aging. This increase was confirmed by optical microscopy and x-ray diffraction to be due to martensite formation.

It is anticipated that subsequent return to service temperature of a microstructure with martensite may alter the expected aging characteristics of this alloy. To the author's knowledge, this has not been investigated. Although normal martensite reversion to austenite is expected, it is postulated that the high diffusion rates permitted by the body-centred tetragonal (BCT) structure may allow accelerated transformation to sigma or other intermetallic phases. It is furthermore proposed [9] that reactions involving large-scale atomic transformations, such as to martensite, may assist in sigma-phase nucleation.

Experimental

Microstructural changes occurring during simulated service at 750°C were investigated for weld metal of three different compositions within the SFA-5.9 composition range. The compositions are summarized in Table 1 and covered commercially available compositions of lean and high alloyed compositions, respectively identified as C1 and C3. A third composition, C2, targeting the minimum limits of SFA-5.9 was experimentally prepared by controlled dilution of commercial 16-8-2 wire with ER80S-B8. The weld metal was deposited by gas–metal arc welding as a V-groove butt weld on 35 mm thick SA-240 Gr 304H base material, as depicted in Figure 1. Typical parameters employed during welding were as follows:

- Shielding Gas: 98%Ar-2%CO_2
- Arc Current: 190 – 210 A
- Arc Voltage: 21 – 25 V
- Travel Speed: 215 – 225 mm/min (maintained using mechanised welding)
- Calculated Arc Energy: 1.2 – 1.4 kJ/mm

Table 1: Chemical compositions of weld metals (mass%)

	Composition C1 (Lean Commercial)	**Composition C2** (Lean Experimental)	**Composition C3** (High-Alloy Commercial)
C	0.06	0.07	0.06
Cr	15.3	14.4	16.2
Mo	1.2	1.1	1.3
Ni	8.2	7.8	9.4
Mn	1.4	1.4	1.4
Si	0.5	0.5	0.5
Cu	0.05	0.05	0.2
Predicted Parameters			
Ferrite content (FN) (WRC-1992)	~1	~0	~2
M_s (°C) Self et al. [15]	−49	−21	−126
M_s (°C) Self et al. [15] (excluding carbide term)	−71	−49	−150

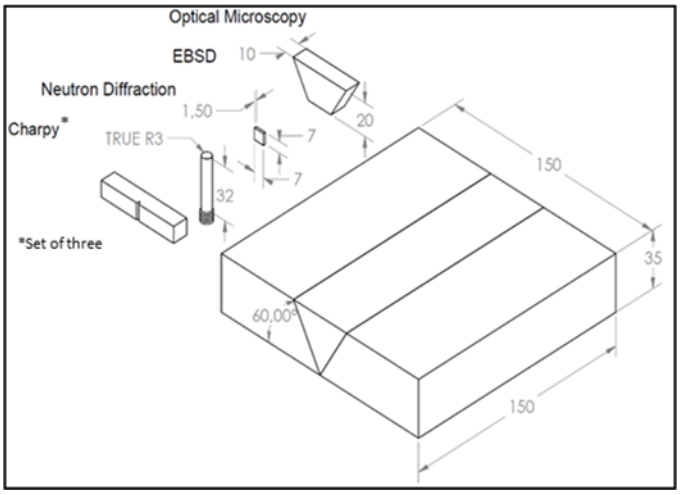

Figure 1 Schematic depiction of weld coupons with sample dimensions and orientations of samples extracted from the coupons. Dimensions are reported in millimeters

The elevated-temperature behaviour was evaluated in two phases. In the first phase, the formation of martensite was evaluated by single-cycle exposure to 750°C for durations varying between 10 h and 3500 h. In the second phase, martensite was intentionally formed by cooling samples to ambient temperature after 1000 h exposure to 750°C. The samples were subsequently returned to 750°C for durations of 300 h and 2500 h. All the abovementioned samples were subjected to cooling in still air following elevated temperature exposure.

The influence of the abovementioned thermal simulations was evaluated by several analytical destructive and non-destructive test methods. The total content of ferromagnetic phases (comprising ferrite and α'-martensite) was measured using a Fischer FMP30 Feritscope: averages of five measurements are reported. In order to limit the effects of base metal dilution, all measurements were taken in cross-section within 20 mm from the cap surface and at least 10 mm away from either fusion line. All samples for destructive tests were extracted from the weld metal using wire erosion: the dimensions and orientations are depicted in Figure 1.

Neutron diffraction evaluation was performed at the SAFARI-1 reactor of the South African Nuclear Energy Corporation. Samples were analysed at room temperature, −15°C, and −30°C. Diffraction data were analysed using the Rietveld least-squares method, in which measured patterns were compared with calculated diffraction patterns for the respective expected phases (produced using GSAS II software). The relative contributions of austenite (face-centred cubic; FCC) and ferrite (body-centred cubic; BCC) to the measured diffraction pattern (after performing background correction) were established to quantify the amount of each phase present in the sample.

Samples for electron backscatter diffraction (EBSD) were prepared by grinding to a 15 micron finish followed by electropolishing with a Struers Electropol 5 instrument employing Struers A3 electrolyte (comprising mainly perchloric acid) at 30 V for 30 s. EBSD accompanied by elemental mapping using energy-dispersive X-ray spectroscopy (EDS) was performed using a JEOL JSM700F field-emission scanning electron microscope (FEG-SEM). Oxford AZtechHKL EBSD software (version 3.3) was used for the acquisition and analysis of the EBSD (Kikuchi) patterns. Transmission electron microscopy (TEM) was performed using a Jeol JEM-2100. Because this study focussed on the behaviour of lean variants during aging, the higher-alloyed composition (C3) was not subjected to EBSD and TEM evaluation.

Impact testing was performed at −30°C in accordance with ASTM A370 [10]: average values of three results are reported for each condition. Metallography was performed following etching with oxalic acid, KOH, and Marble's reagent.

Results

The change in the apparent ferrite content (constituting delta ferrite and α'-martensite), as measured by Feritscope, is depicted in Table 2. Although a direct translation from FN to percentage ferrite is not truly correct, a 1:1 equivalence is often accepted for such low values [11]. The results confirmed relatively good correlation between the ferrite content predicted from the WRC-1992 diagram and the actual measured values in the as-welded condition. The two lean variants (C1 and C2) demonstrated significant increases in apparent ferrite content, which reached maxima at 1000 h of aging at 750°C. Thereafter, the apparent ferrite content decreased with aging time. The leanest variant (C2) demonstrated the greatest increase in apparent ferrite content. Conversely, the higher-alloyed variant (C3) demonstrated a steady decline in apparent ferrite content, with almost no ferrite being magnetically detectable after 3500 h of aging.

Table 2: Comparison of apparent ferrite content, as measured using a Fischer® Feritscope, after exposure to 750°C. Reported ranges represent the 95% confidence interval.

Exposure time	**C1** (Lean Commercial)	**C2** (Lean Experimental)	**C3** (Higher-alloyed Commercial)
Predicted ferrite content (FN) (WRC-1992)	~1	~0	~2
As-welded	0.9 ± 0.4	1.0 ± 0.2	2.4 ± 0.3
10 h	1.6 ± 0.6	3.4 ± 0.5	-
100h	2.3 ± 0.2	7.4 ± 1.2	-
1000 h	10.1 ± 6.0	24.4 ± 6.3	0.7 ± 0.1
1000 h → air cool → 300 h	6.5 ± 1.5	18.0 ± 14.2	0.2 ± 0.1
1300 h	7.4 ± 1.9	21.4 ± 9.2	0.3 ± 0.16
1000 h → air cool → 2500 h	0.5 ± 0.4	10.4 ± 7.2	0.1 ± 0.1
3500 h	4.4 ± 1.8	15 ± 11.9	0.02 ± 0.04

Samples that were intentionally cooled to ambient after 1000 h of aging and then returned to 750°C were also characterised. An additional 300 h of aging significantly reduced the apparent ferrite content compared with the results for a single 1000 h exposure. A greater decrease in apparent ferrite content was noted when the subsequent aging time after cooling to ambient was increased from 300 h to 2500 h.

The neutron diffraction results (Table 3) at ambient temperature reported total BCC concentrations similar (within statistical variance) to those measured magnetically by means of the Feritscope. The results also indicate that cooling of the lean experimental composition (C2) in the as-welded condition to −30°C had no significant influence on the BCC content. Conversely, samples aged at 750°C for 1000 h demonstrated a significant increase in BCC content when cooled from ambient to −15°C, although there was no further change on temperature decrease to −30°C. The BCC content did not change upon return to ambient temperature.

Table 3: Results from neutron diffraction evaluation performed at various temperatures. The values represent the ferrite content expressed as mass %.

Aged Condition	**Test Temperature**	**C1** (Lean Commercial)	**C2** (Lean Experimental)
As-welded	Ambient (22°C)	Results not available	0.3
	−15°C		0.7
	−30°C		0.6
	Ambient (after exposure to −30°C)		0.6
1000 h @ 750°C	Ambient (22°C)	7.0	17.2
	−15°C	28.4	35.1
	−30°C	24.7	33.6
	Ambient (after exposure to −30°C)	29.7	34.0

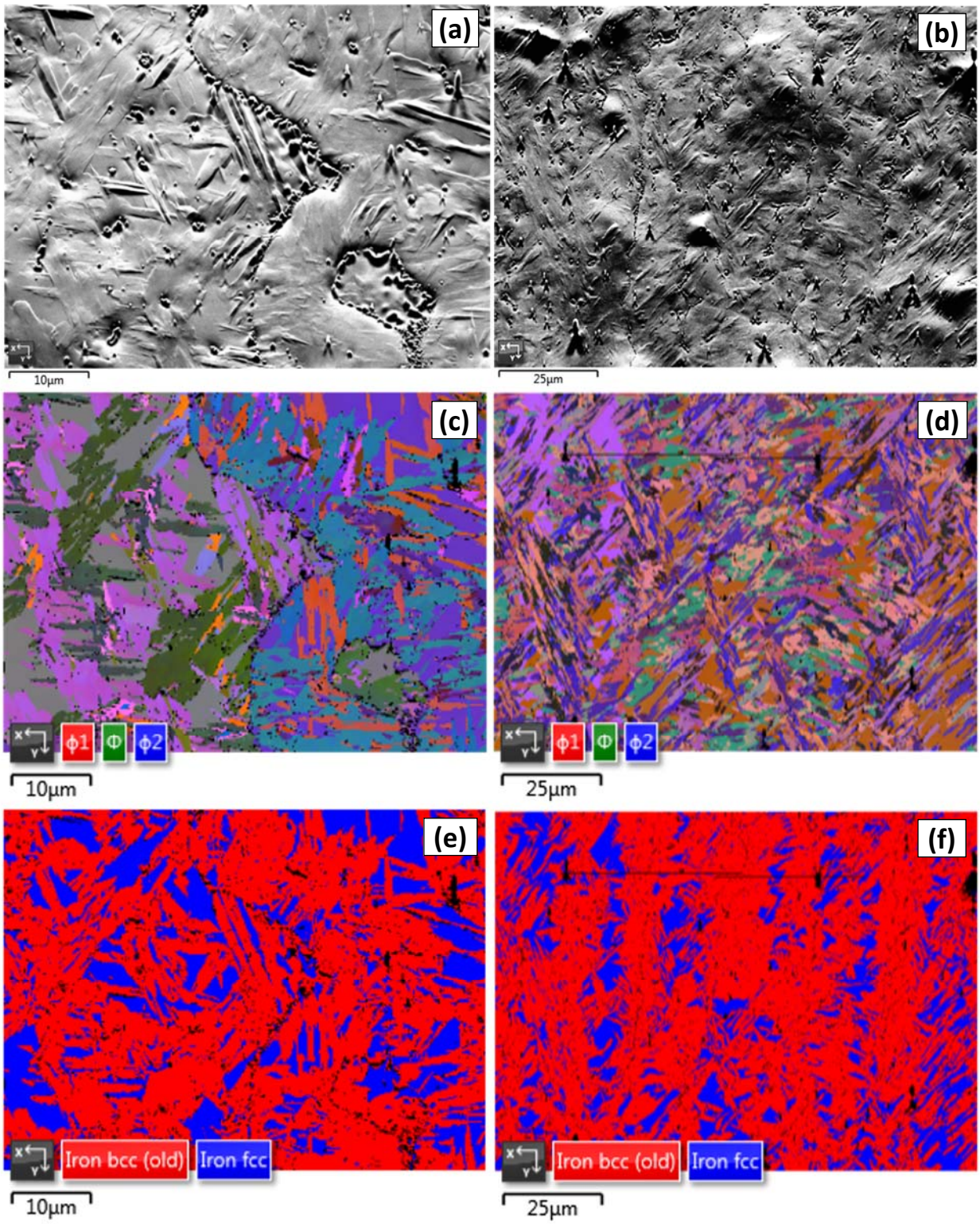

Figure 2 Electron backscatter diffraction results from samples C1 (left) and C2 (right) after aging at 750°C for 1000 h. (a) and (b): electron micrograph showing precipitates on grain boundaries surrounded by needle-like phases. (c) and (d): orientation of respective phases presented on a Euler diagram. (e) and (f): phase map

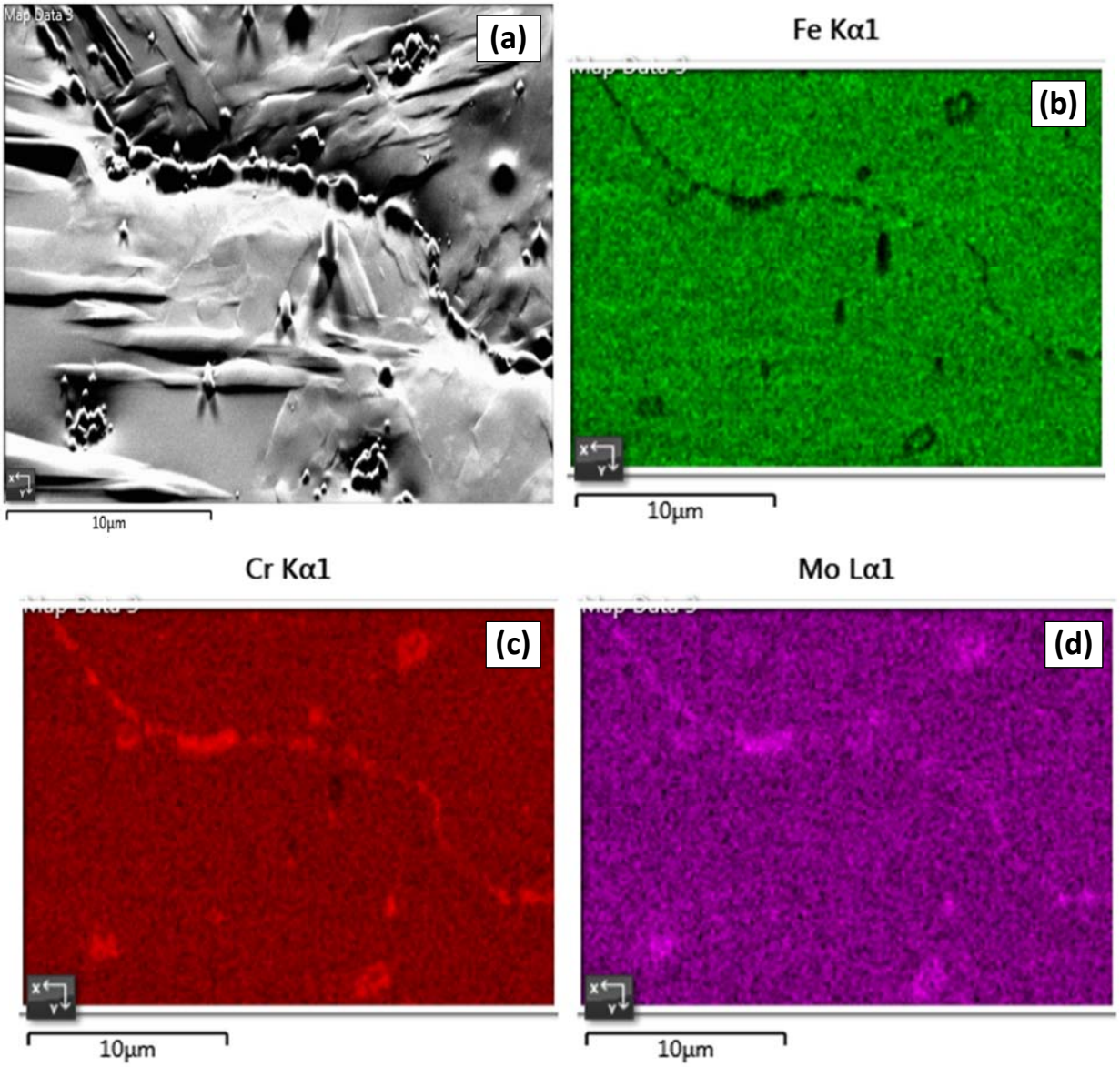

Figure 3 (a) Electron micrograph of higher magnification view of lean commercial sample C1 after aging at 750°C for 1000 h. Elemental mapping via energy-dispersive spectroscopy of (b) Fe, (c) Cr, and (d) Mo

Scanning electron microscopy of the two lean variants (C1 and C2) revealed microstructures comprising grain boundary precipitates with numerous plate-like phases protruding from the grain boundaries into the austenitic matrix (Figure 2). EBSD identified the plate-like phases to match the Kikuchi patterns for BCC ferrite. Euler diagrams also hinted at the existence of a preferential orientation relationship between the ferrite plates and the austenitic matrix (due to similarity in colours of ferrite plates) (Figure 2). No intermetallic phases were identified in this evaluation. Elemental mapping identified the intergranular precipitates as highly enriched in the carbide-forming elements, Cr and Mo, and depleted in Fe and Ni contents (Figure 3). The elemental mapping furthermore indicates that there was no major composition difference between the BCC plates and the austenitic matrix.

The observed microstructure was extremely fine; therefore, limited information could be obtained by optical microscopy due to magnification limitations. All three compositions in the as-welded condition contained microstructures consisting primarily of austenite, with small discontinuous areas of delta ferrite. No intermetallic

phases could be discerned. Each of the three compositions aged for total durations of 1000 h and longer revealed the presence of intergranular carbides. Delta ferrite was additionally found to have decomposed into secondary austenite and carbides on the austenite–ferrite boundary. Figure 4 shows an electron micrograph of decomposed delta ferrite and associated grain boundary carbides for the lean commercial composition (C1) after aging for 1000 h at 750°C. No intermetallic phases, such as sigma or laves phases, could be discerned in the aged condition.

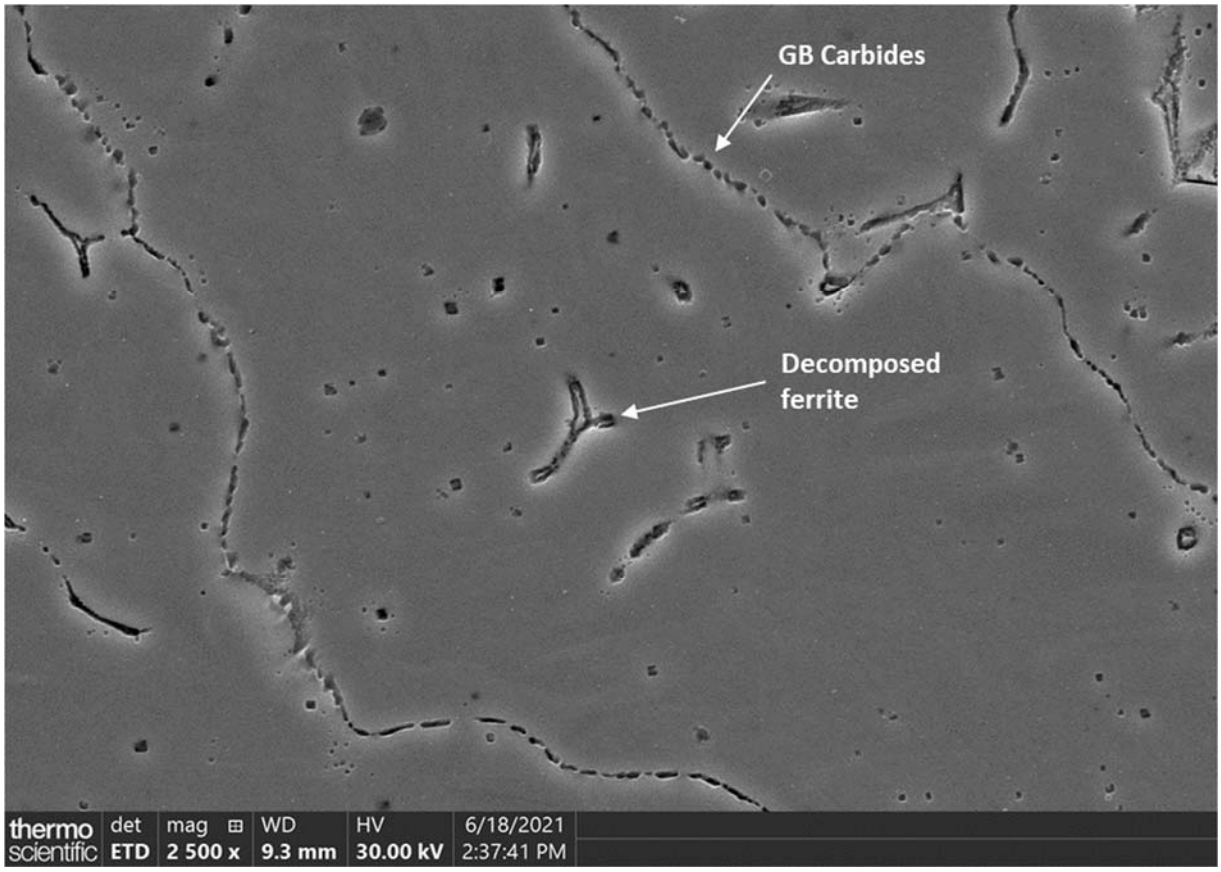

Figure 4 Scanning electron micrograph of lean commercial composition C1 after aging at 750°C for 1000 h (etched in oxalic acid)

Thin-film TEM allowed for accurate measurement of the chemical composition of selected precipitates with EDS due to its limited interaction with underlying material. Figure 5 shows a TEM micrograph of the lean commercial composition (C1) after exposure to 750°C for 1000 h. Grain-boundary precipitates are observed. The corresponding compositions at each of the positions marked in Figure 5 are reported in Table 4. $M_{23}C_6$-type carbides formed in 316 stainless steel were reported [12] to contain 63% Cr, 18% Fe, 14% Mo, and 5% Ni. This composition is very close to that of the grain-boundary precipitates evaluated in Figure 5 and Table 4: the precipitates were therefore identified as $M_{23}C_6$ carbides.

Impact test results measured at −30°C are summarized in Figure 6. Taking cognizance of the fact that limited information can be deduced from impact energies at a single test temperature, several relevant observations can still be made. The highest energies were displayed in the as-welded condition; aging reduced the impact energies for all compositions. The leanest variant (C2) experienced the greatest reduction in impact energy, whereas the higher-alloyed variant (C3) experienced the lowest reduction in impact energy.

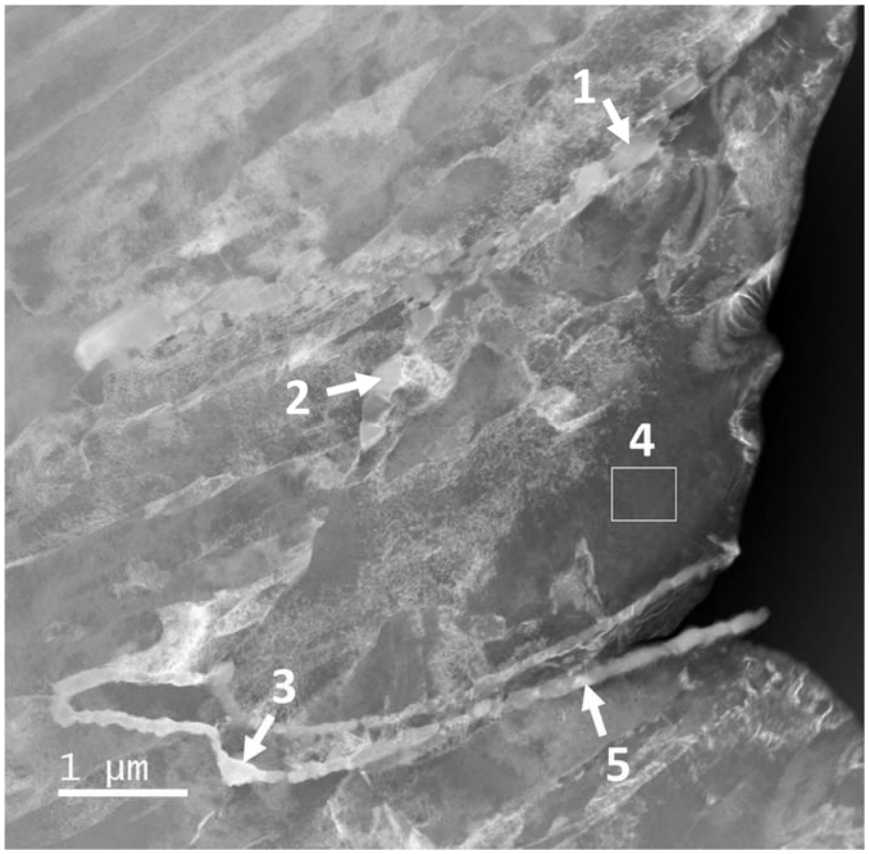

Figure 5 Transmission electron micrograph of lean commercial composition C1 after exposure to 750°C for 1000 h, indicating grain-boundary precipitates and positions where elemental spot analyses were performed. Measured compositions are reported in Table 4

Table 4: Chemical composition (mass %) as determined by EDS of selected areas identified on Figure 5. Reference is also made to the measured composition of $M_{23}C_6$ in an aged 316 alloy [12].

	Position 1 (Boundary precipitate)	**Position 2** (Boundary precipitate)	**Position 3** (Boundary precipitate)	**Position 4** (Matrix)	**Position 5** (Boundary precipitate)	$M_{23}C_6$ composition in 316 [12]
Fe	16.5	16.9	25.7	75.2	15.7	18
Cr	69.7	69.9	61.7	16.4	67.6	63
Mo	11.7	10.9	10.2	1.3	14.4	14
Ni	1.4	1.4	1.9	5.8	0.9	5
Mn	0.8	0.9	0.4	1.3	1.4	(not reported)

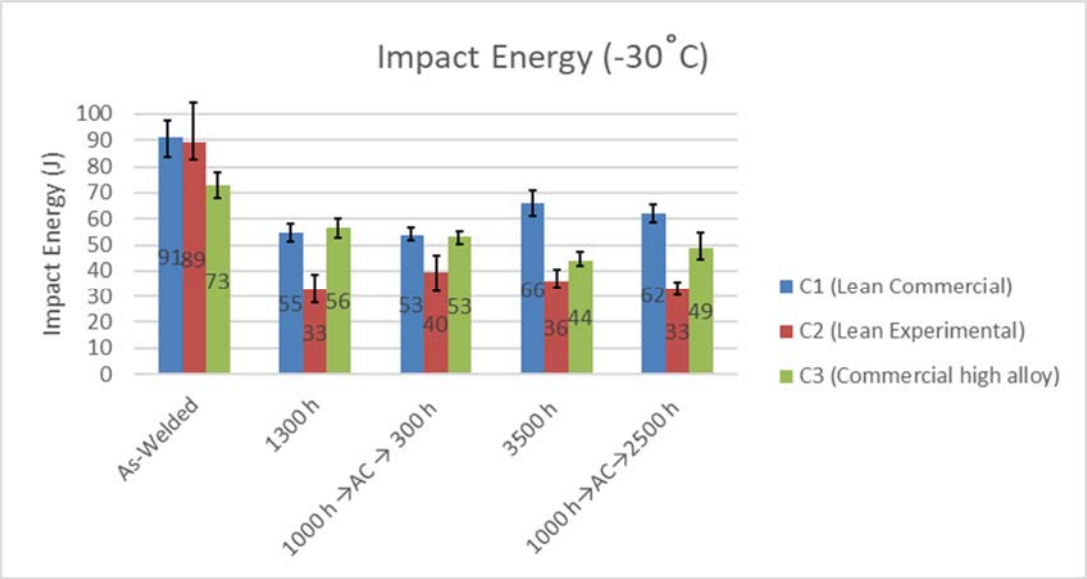

Figure 6 Average impact test results at −30°C for the three compositions of weld metals for different aged conditions. Error bars represent minimum and maximum test values.

Discussion

The low delta ferrite content in the as-welded condition, as is characteristic for type 16-8-2 weld metal, is corroborated by the magnetic, neutron diffraction, and microscopic evaluations performed in this work. The ferrite content was, however, significantly altered during exposure to 750°C for various durations. It is critical to observe that both delta ferrite and α'-martensite are ferromagnetic: the apparent ferrite content reported from Feritscope measurements therefore represents the combined concentrations of these phases. Similarly, α'-martensite has a BCT crystal structure. The low carbon content, however, results in a very low degree of tetragonality and it is therefore detected in diffraction studies with a Kikuchi pattern matching that of BCC ferrite. The absence of a chemical composition difference between the austenitic matrix and the BCC plates (as demonstrated in Figure 3) was consistent with the fact that the martensitic transformation is diffusionless.

Conventional austenitic stainless-steel weld metals normally demonstrate a reduction in ferrite content during elevated-temperature exposure [7, 8, 13]. This is caused by the transformation of delta ferrite into non-magnetic phases constituting either a combination of secondary austenite and $M_{23}C_6$ carbides or sigma phase [14]. Hsiao [13] found that aging of 16-8-2 weld metal at 650°C for 672 h only resulted in ferrite decomposing into a combination of austenite and carbides. It is noted that the weld metal used in his study was higher alloyed (16.8%Cr, 9.3%Ni and 2%Mo) and thus closer in composition to variant C3. This behaviour was demonstrated in the higher-alloyed variant (C3) evaluated in this work, where a constant reduction in ferrite content was measured with increasing elevated temperature and aging duration. Figure 7 indicates that essentially only austenite and approximately 1.2% $M_{23}C_6$ carbides are thermodynamically stable at 750°C in an alloy of bulk composition equivalent to that of the lean commercial variant (C1). A similar delta ferrite decomposition is therefore expected with aging, as observed with the higher-alloyed variant (C3). Both lean variants, however, demonstrated contradictory behaviour, with a significant increase in apparent ferrite content. Delta ferrite decomposition during aging was metallographically observed for all three compositions, so the increase in apparent ferrite content is attributed to the formation of martensite. Grain-boundary precipitates with composition consistent with that expected for $M_{23}C_6$ were formed during aging at 750°C. It is therefore deduced that the associated sensitization of the austenitic matrix locally raised the M_s temperature above ambient and so martensite formed during cooling. Figures 2 and 3 provide evidence of this reaction due to the presence of martensite plates adjacent to grain boundaries containing $M_{23}C_6$ carbides. It is proposed that the width of this zone increased with aging duration up

to a maximum of 1000 h; aging beyond 1000 h resulted in back-diffusion of solute from the adjacent austenitic matrix, which again lowered the M_s temperature to below ambient.

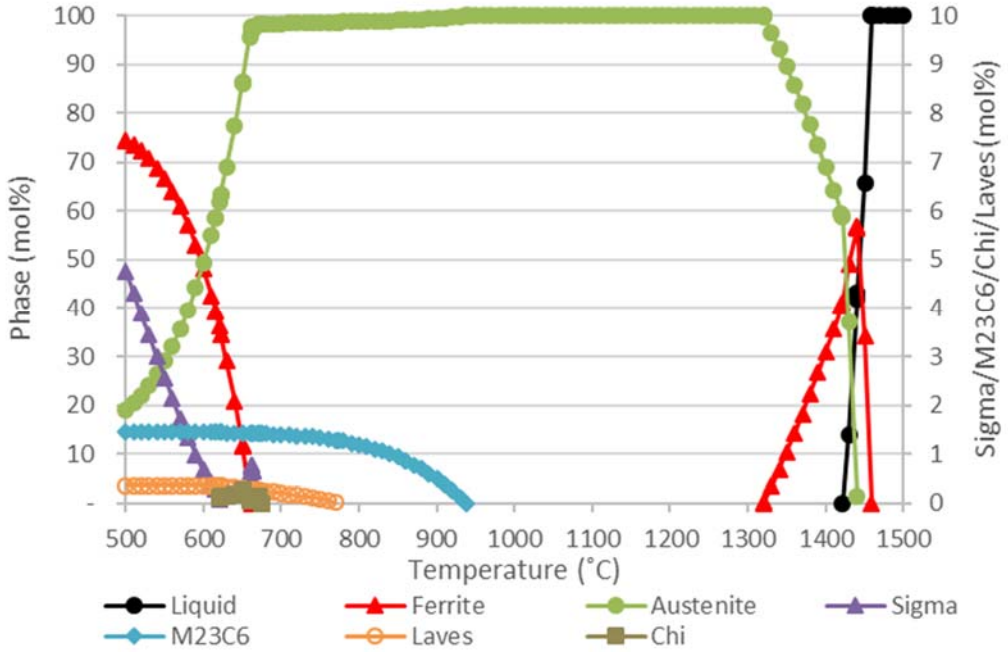

Figure 7 Thermodynamically stable phases for a uniform weld metal of composition equivalent to that of lean commercial alloy C1, as predicted using Thermo-calc software

Neutron diffraction results of the lean experimental composition (C2) in the as-welded condition suggested that the M_s temperature is well below −30°C because a negligible change in apparent ferrite content occurred when analysed at this temperature. The prediction of M_s value proposed by Self et al. [15] includes a term that compensates for an increase in M_s due to carbide formation. Table 1 indicates a predicted M_s temperature for C2 of −49°C when this term is excluded (as would be the case for the as-welded condition), which supports the neutron diffraction results. The predicted M_s temperatures in the aged condition (i.e., with the carbide term included) for the two lean compositions are −21°C and −49°C, respectively. The actual onset of martensite formation was, however, observed to occur above ambient temperature when these alloys were aged at 750°C for 1000 h. More martensite formed when these two aged alloys were cooled from ambient to −15°C, but no further increase in martensite formation occurred on subsequent cooling to −30°C. It is therefore concluded that the sensitized regions of the austenitic matrix were completely transformed to martensite at −15°C and that the M_s temperature for the remaining matrix was probably well below −30°C. Relying solely on the commonly used empirical equations for prediction of the M_s temperature in these lean alloys in the aged condition may therefore be misleading. This is in line with the conclusion drawn by Michler [16] with respect to slightly higher-alloyed 308 weld metals. The implication is, however, more important for lean type 16-8-2 weld metals due to the presence of the martensite transformation at ambient temperature (as opposed to cryogenic temperatures for higher-alloyed weld metals). The use of more accurate, yet complex, thermodynamic models for prediction of the M_s temperature may be considered if it is able to compensate for local concentration gradients associated with sensitisation.

The abovementioned reaction and observations are consistent with prior findings [7, 13, 17]. Hsiao [13] measured the ferrite content by magnetic means during strain of 16-8-2 weld metals and reported that metals that received prior aging treatment of 0.5 h at 880°C experienced a significant increase in apparent ferrite content with increasing strain. This was ascribed to strain-induced martensite formation. This behaviour was much less prominent during strain of 16-8-2 weld metal in the as-welded condition. As indicated earlier, the weld metal used by Hsiao [13] was higher alloyed than conventional 16-8-2. This therefore explains why martensite could only be

formed with prior aging and subsequent straining. Marshall and Farrar [7] found that type 16-8-2 weld metal aged at 750°C for 5 h experienced an increase in apparent ferrite content from 3 FN in the as-welded condition to well over 17 FN. The influence of sensitisation on martensite formation was well demonstrated and explained by Butler and Burke [17], who studied martensite formation adjacent to grain boundaries of sensitised 304 stainless steel during cryogenic cooling. Concentration gradients established during sensitisation were measured and the associated increase in M_s temperatures calculated in these local areas.

The maximum amount of martensite to form during cooling to −15°C appears to be slightly larger for the lean experimental alloy (C2) compared with the lean commercial alloy (C1). This is ascribed to a combination of a lower bulk M_s temperature (due to its inherently lower total alloying content) as well as slightly higher C content. The maximum amount of $M_{23}C_6$ carbide that can form is limited by the C concentration. The formation of greater amounts of carbides results in removal of more Cr and Mo from the austenitic matrix, thus raising the M_s over a wider diffusion distance and allowing for the formation of greater amounts of martensite.

The occurrence of martensitic transformation after aging of type 16-8-2 weld metal of leaner targeted composition is proven and characterized in the aforementioned discussion and in literature. Of further interest is how the formation of martensite in these weld metals will affect microstructural changes during subsequent return to elevated-temperature service (as would be the case for re-commissioning elevated-temperature equipment). The data presented in Table 2 indicate that the amount of martensite formed in the two lean variants during cooling after aging for 1000 h at 750°C was reduced during subsequent aging at 750°C. This suggests martensite reversion to the thermodynamically more stable austenite during aging (refer Figure 7). This reversion appears to be time-based and significantly less martensite was remnant after 2500 h of aging compared with aging for 300 h. Ghosh [18] confirmed that such martensite reversion is diffusion-based, which supports this observation. Furthermore, it is interesting to note that samples with an interrupted cooling cycle at 1000 h also experienced a greater decrease in martensite content during subsequent aging when compared with those of the same composition aged in a single cycle for the same total duration (e.g., 1000 h → air cool → 2500 h compared with 3500 h). This difference stems from the fact that the underlying mechanisms causing the reduction differ: in the case of single-cycle exposure, the decrease in martensite content is attributed to repair of a sensitized matrix through diffusion; in multiple cycles, this observation is attributed to martensite reversion. Interim martensite formation could not be confirmed to influence susceptibility to subsequent formation of sigma and other intermetallic phases because no such phases were detected despite extended period of elevated temperature exposure. Al Dawood et al. [19] reported formation of laves phase during martensite reversion at 650°C in an alloy containing 16% Cr, 5% Ni, and 1% Mo. At higher temperatures, this was associated with intergranular $M_{23}C_6$ formation in addition to martensite reversion.

The reduction in impact energy for all aging treatments is consistent with the expectation for most conventional austenitic stainless-steel weld metals primarily due in intergranular carbide formation. Marshall and Farrar [7] proposed that the presence of martensite in 16-8-2 weld metals is not detrimental to the fracture properties and that it may have a beneficial transformation-induced plasticity effect. In the current work, the larger reduction in impact energy for the two lean variants (C1 and C2) as compared to the higher alloyed variant (C3) is ascribed to the formation of martensite. Although martensite contains little carbon, and thus is expected not to cause significant embrittlement, its BCT crystal structure still possesses an inherent ductile-to-brittle transition temperature, which is absent for the austenitic matrix. Carbide formation is solely responsible for the reduction in impact energy with aging for the higher-alloyed sample (C3), whereas that for the leaner variants is ascribed to a combination of carbide formation and the presence of martensite. Overall observation of the impact energies for the aged samples also supports the absence of a significant intermetallic embrittling mechanism (such as the presence of continuous sigma phase). Fink et al [8] observed a reduction in impact energy when 16-8-2 weld metal was exposed to 705°C for 168 h, although the extent was lower than for 308H weld metal wherein delta ferrite transformed into sigma phase. In the current work, it was identified that the amount of martensite which forms after aging influences the reduction in impact energy. As demonstrated in the impact energies for the three different 16-8-2 variants, changes in composition that influence the extent of martensite formation affect the cryogenic impact properties.

Although this work did not conclusively identify a deleterious effect of martensite formation in these alloys, this phenomenon has been proposed by some [12, 13, 20] to negatively influence stress corrosion properties. Further studies are needed to fully elucidate the influence of these alloy compositions on elevated-temperature creep, ductility, and microstructural transformation at operating temperatures below 750°C.

Conclusions

The microstructural changes occurring in type 16-8-2 weld metal of different compositions within the SFA-5.9 specification after elevated temperature exposure for extended times were investigated. The following conclusions were drawn from the results presented in this work:

1. Type 16-8-2 weld metal targeting lean compositions (towards the lower limits of the SFA-5.9 specification for this alloy) are susceptible to the formation of martensite during exposure to 750°C. The formation of martensite cannot accurately be predicted using empirical models derived for the prediction of M_s temperatures in these alloys. The martensite formation is ascribed to the removal of solute elements from the austenitic matrix due to carbide formation that locally raises the M_s to values above ambient temperature.
2. The amount of martensite formed in the lean variants reached a maximum at 1000 h of aging at 750°C. During further extended aging, it decreased due to repair of the sensitized regions via diffusion from the austenitic matrix. Subsequent aging of martensite formed during an initial aging operation resulted in martensite reversion to austenite. The martensite reversion was identified to be time-dependent, with almost complete reversion observed in the lean commercial variant after 2500 h of aging at 750°C. Although the sum of aging durations beyond 1000 h resulted in a reduction in the martensite content, the responsible underlying mechanisms differed for a single high-temperature exposure compared with multiple exposures.
3. The increase in apparent ferrite content due to martensite formation was not observed in the higher-alloyed variant of type 16-8-2 weld metal, in which the ferrite content continuously decreased during aging due to decomposition of delta ferrite into a combination of $M_{23}C_6$ carbides and austenite.
4. The formation of martensite in the lean variants of 16-8-2 was proven to influence the cryogenic impact energy. Whilst an overall reduction in impact energy was observed for all three variants after exposure to 750°C due to carbide formation, the reduction was greater in the leaner variants that contained martensite. The leanest 16-8-2 variant, which formed the greatest amount of martensite after aging, experienced the greatest reduction in impact energy.
5. No intermetallic phases were identified in any of the 16-8-2 weld metal variants despite being exposed to extended aging durations of up to 3500 h. There is therefore no evidence to suggest that the presence of martensite affected intermetallic phase formation during subsequent return to elevated temperature.

Recommendations

The following are recommended if the formation of martensite in a 16-8-2 weld metal is not desired:

- It is not appropriate to specify a minimum calculated M_S temperature as a control limit for type 16-8-2 weld metal because the extent to which the M_s increases during aging is also a function of the chemical composition (principally C). It is preferable to re-evaluate the minimum values of the individual elements (Cr, Ni, Mo, N, Mn) and consider these in conjunction with the C content.
- Newly commissioned high-temperature equipment should not be cooled until after an operating period of at least several thousand hours. This time at elevated temperature was proven sufficient to allow back-diffusion of Cr and Mo to the affected regions and thus avoid martensite formation during subsequent return to ambient temperature.
- It is recommended that a higher Mn content in the alloy be considered. Increasing the concentration of this element lowers the overall M_s temperature yet does not affect the primary ferritic solidification mode and neither does it partake in any elevated-temperature precipitation reaction.

It is further recommended that study of the effect of such martensite formation on elevated-temperature properties be extended to include a wider range of aging temperatures and cover properties such as creep strength and ductility.

Acknowledgements
The authors acknowledge support from Sasol Ltd and the University of Pretoria in the execution of this work. Appreciation is extended to the Nuclear Energy Corporation of South Africa for performing the neutron diffraction analyses, Kelvion Thermal Solutions for welding of the samples, Welding Alloys for donating welding wire to weld sample C3, and the Centre for High Resolution Transmission Electron Microscopy at Nelson Mandela University (South Africa) for performing the EBSD and TEM evaluations. English language editing of this manuscript was carried out by Prof. K. C. Sole.

Declarations

Funding
The experimental portions of this work was funded by Sasol Ltd and the University of Pretoria. Welding work was performed by Kelvion Thermal Solutions (Pty) Ltd and some of the wire was donated by Welding Alloys Ltd.

Conflicts of interest
Not Applicable

Availability of data and material
All supporting research data are transparent and available upon request.

Authors' contributions
Not Applicable. This work was jointly executed by both authors.

References

[1] American Society of Mechanical Engineers (2019) Boiler & pressure vessel code, Section II Part C: Specifications for welding rods, electrodes, and filler metals, SFA-5.9 Annex A
[2] Lundin CD, Delong WT, Spond DF (1975) Ferrite fissuring relationship in austenitic stainless steel weld metals. Weld J 54(8):241s–246s
[3] Carpenter OR, Wylie RD (1956) 16-8-2 Cr-Ni-Mo for Welding Electrode. Metal Progress 70(5):65–73
[4] American Petroleum Institute (2017) Recommended practice 942-B: Material, fabrication, and repair considerations for austenitic alloys subject to embrittlement and cracking in high temperature 565°C to 760°C refinery services
[5] Leitnaker JM (1982) Prevention of chi and sigma phases formation in aged 16-8-2 weld metal. Weld J 61(1) 9s
[6] Kotecki DJ (1999) A Martensite Boundary on the WRC-1992 diagram. Weld J 78 (5):180s–192s
[7] Marshall AW, Farrar JCM (2001) Lean Austenitic Type 16.8.2 Stainless Steel Weld Metal. Stainless Steel World 2001 conference papers 216–222
[8] Fink C, Wang H, Alexandrov BT, Penso J (2020) Filler Metal 16-8-2 for Structural Welds on 304H and 347H Stainless Steels for High-Temperature Service. Weld J 99(12):312s–322s https://doi.org/10.29391/2020.99.029
[9] Vitek JM, David SA (1986) The sigma phase transformation in austenitic stainless steels. Weld J 65(4):106s–111s
[10] American Society for Testing and Materials (2020) A370 Standard test methods and definitions for mechanical testing of steel products
[11] American Welding Society (2006) A4.2 Standard Procedures for calibrating magnetic instruments to measure the delta ferrite content of austenitic and duplex ferritic-austenitic stainless steel weld metal.

[12] Weiss B, Stickler R (1972) Phase instabilities during high temperature exposure of 316 austenitic stainless steel. Metall Trans 3:851–866

[13] Hsiao, Y-H (1994) Factors affecting creep damage accumulation and mechanical properties of 316 stainless steel weldments. PhD Dissertation, Ohio State University

[14] Gill TPS, Vijayalakshmi M, Gnanamoorthy JB, Padmanabhan KA (1986) Transformation of delta-ferrite during the postweld heat treatment of type 316L stainless steel weld metal. Weld J 65(5):122s–128s

[15] Self JA, Olson DL, Edwards GR (1984) A study on the stability of austenitic weld metal. Proceedings IMMCC, Kiev, USSR

[16] Michler T (2007) Formation of martensite in 304 grade stainless steels and their welds. Mat-wiss Werkst Tech 38(1):32–35. https://doi.org/10.1002/mawe.200600052

[17] Butler EP, Burke MG (1986) Chromium depletion and martensite formation at grain boundaries in sensitised austenitic stainless steel. Acta Metall 34(3):557–570

[18] Ghosh SK, Shikhar J, Mallick P, Chattopadhyay PP (2013) Influence of mechanical deformation and annealing on kinetics of martensite in a stainless steel. Materials Manufacturing processes 28(3):249-255. https://doi.org/10.1080/10426914.2012.667893

[19] Al Dawood M, El Mahallawi S, Abd El Azim ME, El Koussy MR (2004) Thermal aging of 16Cr-5Ni-1Mo stainless steel Part 1 – Microstructural analysis. Mat Sci Tech 20:363–369. https://doi.org/10.1179/026708304225011135

[20] Saluja R, Moeed KM (2014) Emphasis of embrittlement characteristics in 304L and 316L austenitic stainless steel. IOSR J Mech Civil Eng 11(6):4–10